



HAL
open science

Quantifying CMIP6 model uncertainties in extreme precipitation projections

Amal John, Hervé Douville, Aurélien Ribes, Pascal Yiou

► **To cite this version:**

Amal John, Hervé Douville, Aurélien Ribes, Pascal Yiou. Quantifying CMIP6 model uncertainties in extreme precipitation projections. 2022. hal-03464913v2

HAL Id: hal-03464913

<https://hal.science/hal-03464913v2>

Preprint submitted on 22 Mar 2022

HAL is a multi-disciplinary open access archive for the deposit and dissemination of scientific research documents, whether they are published or not. The documents may come from teaching and research institutions in France or abroad, or from public or private research centers.

L'archive ouverte pluridisciplinaire **HAL**, est destinée au dépôt et à la diffusion de documents scientifiques de niveau recherche, publiés ou non, émanant des établissements d'enseignement et de recherche français ou étrangers, des laboratoires publics ou privés.

Journal Pre-proof

Quantifying CMIP6 model uncertainties in extreme precipitation projections

Amal John, Hervé Douville, Aurélien Ribes, Pascal Yiou



PII: S2212-0947(22)00023-8
DOI: <https://doi.org/10.1016/j.wace.2022.100435>
Reference: WACE 100435

To appear in: *Weather and Climate Extremes*

Received date: 8 October 2021
Revised date: 9 February 2022
Accepted date: 10 March 2022

Please cite this article as: A. John, H. Douville, A. Ribes et al., Quantifying CMIP6 model uncertainties in extreme precipitation projections. *Weather and Climate Extremes* (2022), doi: <https://doi.org/10.1016/j.wace.2022.100435>.

This is a PDF file of an article that has undergone enhancements after acceptance, such as the addition of a cover page and metadata, and formatting for readability, but it is not yet the definitive version of record. This version will undergo additional copyediting, typesetting and review before it is published in its final form, but we are providing this version to give early visibility of the article. Please note that, during the production process, errors may be discovered which could affect the content, and all legal disclaimers that apply to the journal pertain.

© 2022 Published by Elsevier B.V. This is an open access article under the CC BY-NC-ND license (<http://creativecommons.org/licenses/by-nc-nd/4.0/>).

Quantifying CMIP6 model uncertainties in extreme precipitation projections.

Amal John ^{*a c}, Hervé Douville^a, Aurélien Ribes^a and Pascal Yiou^b

^aCentre National de Recherches Météorologiques, Météo-France, CNRS, Toulouse,
France

^bLaboratoire des Sciences du Climat et de l'Environnement, UMR 8212
CEA-CNRS-UVSQ, IPSL & U Paris-Saclay, 91191 Gif-sur-Yvette, France

^cUniversité de Toulouse, France

October 2021

*Corresponding Author

DESR/CNRM/GMGEC/CLIMSTAT

CNRM/Météo-France

42, avenue Gaspard Coriolis

Toulouse, 31100, France

john.amal@meteo.fr

Abstract

Projected changes in precipitation extremes and their uncertainties are evaluated using an ensemble of global climate models from phase 6 of the Coupled Model Intercomparison Project (CMIP). They are scaled by corresponding changes either in global mean surface temperature (ΔGSAT) or in local surface temperature (ΔT) and are expressed in terms of 20-yr return values (RV20) of annual maximum one-day precipitation. Our main objective is to quantify the model response uncertainty and to highlight the regions where changes may not be consistent with the widely used assumption of a Clausius-Clapeyron (CC) rate of $\approx 7\%/K$. When using a single realization for each model, as in the latest report from the Intergovernmental Panel on Climate Change (IPCC), the assessed inter-model spread includes both model uncertainty and internal variability, which can be however assessed separately using a large ensemble. Despite the overestimated inter-model spread, our results show a robust enhancement of extreme precipitation with more than 90% of models simulating an increase of RV20. Moreover, this increase is consistent with the CC rate of $\approx 7\%/K$ over about 83% of the global land domain when scaled by (ΔGSAT). Our results also advocate for producing multiple single model initial condition ensembles in the next CMIP projections, to better filter internal variability out in estimating the response of extreme events.

Keywords Climate change, Precipitation, Uncertainty, Extremes

1 Introduction

Global climate models provide an increasingly comprehensive representation of the climate system and are used as a primary tool for understanding and projecting changes in climate mean, variability and extremes due to human activities. The Intergovernmental Panel on Climate Change (IPCC) in its sixth assessment report (AR6) has re-estimated an increase in the observed global mean surface temperature of 1.09°C in 2011–2020 relative to the beginning of the industrial revolution (1850-1900), which can be fully attributed to a human influence (IPCC AR6 SPM Masson-Delmotte et al. (2021)). This anthropogenic global warming is reckoned to have long-term consequences on all components of the climate system, including changes in the daily precipitation distribution. Several generations of multi-model simulations contributing to the Coupled Model In-

38 tercomparison Project (CMIP), supported by observational evidence, show that both the frequency
39 and intensity of extreme daily precipitation events have increased over recent decades (Allen and
40 Ingram, 2002; Asadih and Krakauer, 2015; Scherrer et al., 2016; Karl and Easterling, 1999; Kharin
41 et al., 2013; Min et al., 2011; O’Gorman, 2015). This is also documented in the IPCC special re-
42 port on Managing the Risks of Extremes Events to Advance Climate Change Adaptation (SREX,
43 Seneviratne (2012)).

44 In the absence of moisture limitation and of significant dynamical response, the extreme
45 precipitation intensity is expected to increase exponentially with the atmospheric temperature at
46 a rate determined by the Clausius–Clapeyron (CC) relationship. A robust scaling of daily precipi-
47 tation extremes with global warming across scenarios was confirmed by Li et al. (2020) who found
48 that changes in precipitation extremes follow changes in global warming at roughly the CC rate of
49 $\approx 7\%/^{\circ}\text{C}$ in the latest-generation CMIP6 models. Several studies based on climate model simula-
50 tions show a future increase of precipitation extremes with temperature at a rate comparable to or
51 higher than the CC rate (Li et al., 2020; Kharin et al., 2007; Pall et al., 2007; Allan and Soden,
52 2008; Sugiyama et al., 2010; Kao and Ganguly, 2011; Muller et al., 2011). However, wet extremes
53 are not expected to intensify in all regions (Trenberth, 2011; Pfahl et al., 2017).

54 All these studies either show the multi-model mean or median and have not yet assessed the
55 uncertainties in global CMIP6 projections. A suite of different model projections often exhibits a
56 large spread (Lehner et al., 2020) and can even disagree on a particular region becoming wetter or
57 drier (sign change in the future). Even where there is an overall consensus among the models on the
58 sign of changes in the projected extremes due to a warmer climate, the magnitude of such changes
59 can differ considerably. Though the climate models have improved over recent decades (Wyser
60 et al., 2020; Zelinka et al., 2020), these improvements do not necessarily result in a reduced spread
61 among the projections (Douville et al., 2021). Thus, the main focus of this paper is to quantify the
62 model uncertainties in extreme precipitation projections based on CMIP6 models. We also aim to
63 provide a blueprint on using these projections to identify regions where the projected changes in
64 daily precipitation extremes are consistent with the CC rate and those where they are not.

65 Changes in extreme precipitation against a backdrop of warming climate arise both due
66 to thermodynamic and dynamic effects (Pfahl et al., 2017). A sub-CC relation or even negative
67 dependence on global mean temperature has been found for precipitation extremes over some re-
68 gions, especially over the climatologically dry oceanic regions in the subtropics, presumably as a
69 result of decreasing moisture availability and enhanced large-scale subsidence (Berg et al., 2009;
70 Hardwick Jones et al., 2010; Utsumi et al., 2011; Pfahl et al., 2017). But the question of an ap-
71 propriate choice of temperature for scaling extreme precipitation is still an open question and the
72 available studies differ in scope (Zhang et al., 2019; Schroer and Kirchengast, 2018; Sun et al.,
73 2021). There is a large-scale warming contrast between the continental landmass and the oceans
74 with certain regions over the ocean experiencing a negligible or limited change in the projected
75 surface temperature. The larger warming observed over land may result in a lower scaling with
76 local mean temperature, which may not be considered as a sub-CC scaling rate (Wang et al., 2017).
77 Any departure from the CC rate can be an indication of a dynamical response which may be either
78 amplified or offset by a thermodynamic response regionally (Pfahl et al., 2017; Sherwood et al.,
79 2010; O’Gorman, 2015). Thus here we explore changes in extreme precipitation simply scaled by
80 either global mean or local surface air temperature changes.

81 Several studies (Alexander et al., 2006; Tebaldi et al., 2006; Sillmann et al., 2013a,b) have
82 used various indices as a proxy for different features of precipitation extremes. Here we focus on
83 extreme events with typical return periods of 20 years (or 20-year return values, RV20) as estimated
84 from the annual maximum one-day precipitation (RX1DAY). Projected long-period RX1DAY return
85 value changes are larger than changes in mean RX1DAY and increase with increasing rarity (Mizuta
86 and Endo, 2020; Wehner, 2020). Here we did not explore longer (e.g., 50 or 100 years) return periods
87 since the associated uncertainties would be even stronger than for our RV20 estimations due to the
88 limited sampling.

89 The goal of this study is to assess the uncertainties of projected changes in extreme pre-
90 cipitation based on the multi-model CMIP6 ensemble, to discuss the limitations of assessing the
91 inter-model spread using such ensembles of opportunity, and to highlight the regions where pro-
92 jected changes may not be consistent with the widely used assumption of a Clausius-Clapeyron

93 rate of $\approx 7\%/K$ (Kharin et al., 2013; Westra et al., 2013; Seneviratne et al., 2021). For this pur-
94 pose, we use the SSP5-8.5 scenario from 35 CMIP6 models. The total spread in this ensemble is
95 therefore a combination of both model response uncertainty and internal variability. Therefore, we
96 also assess the potential contribution of internal variability to the inter-model spread by analyzing
97 the projected changes of the RV20 in the CanESM5 model with 25 realizations, with the same
98 concentration scenario.

99 The rest of the paper is structured as follows. We start by introducing in section 2 the models
100 and methods used in this study. Turning to the results in section 3, we address the uncertainties in
101 the model projections along with a discussion on the role of internal variability using the ensemble
102 simulations from CanESM5. The role of local versus global temperature scaling is also assessed.
103 Section 4 summarises the main findings. Other supporting figures and tables are available in the
104 online supplementary material.

105 **2 Data and methods**

106 **2.1 Data**

107 Daily precipitation data from 35 global climate models from the CMIP6 repositories (Eyring
108 et al., 2016) are used in this study. We combine the historical simulations (1850-2014) with one
109 shared socioeconomic pathways (SSPs) projections (O'Neill et al., 2016) running from 2015 to
110 2100. The "end of the road" scenario SSP5-8.5 with the highest emissions is used to get maximum
111 climate change signals and, therefore, better isolate the forced RX1DAY response from internal
112 variability without using large initial condition ensembles (which are only available for a limited
113 number of models). We use the one-model-one-vote approach i.e., without giving any particular
114 weights, although there are inter-dependencies across models (eg Knutti and Masson (2013); Bador
115 et al. (2018)). For each available CMIP6 model, only one member of the historical and SSP5-8.5
116 simulations are used — a treatment that is consistent with the recent IPCC AR6, and which ensures
117 that all models are treated equally. As the total uncertainty in the projected changes is the sum of
118 both model uncertainties and internal climate variability, we here also analyze a single model initial
119 condition large ensemble, provided by the CanESM5 model (Swart et al., 2019), with 25 individual

120 members. Hence we can quantify an upper bound for the total uncertainties.

121 2.2 Climate extreme indices and GEV analysis

122 We first interpolate the daily precipitation data for each model onto a $1^\circ \times 1^\circ$ grid using a first-
 123 order conservative remapping. This allows us to compare multiple models with different resolutions
 124 (typically $1-2^\circ$). For each model, grid point and year, we calculate the annual maximum daily
 125 precipitation (RX1DAY), which is a widely used extreme index defined by the expert group on
 126 Climate Change Detection and Indices (ETCCDI) (Karl et al., 1999; Peterson et al., 2001).

127 We then analyze changes in the return values of RX1DAY, in line with some previous studies
 128 of Kharin et al. (2013) and Wehner et al. (2020). To estimate the 20-year return values, we modeled
 129 the annual maxima of precipitation at each grid point using a nonstationary Generalized Extreme
 130 Value (GEV) distribution using $\log(\text{CO}_2)$ as the co-variate for both the location and scale parameters
 131 (Coles et al., 2001). The parameters are fitted using the Maximum Likelihood Estimate technique
 132 (Easterling et al., 2016). $\log(\text{CO}_2)$ is used as a single co-variate since it has long been recognized to
 133 dominate the world mean temperature projections (Arrhenius, 1896) and allows us to use a common
 134 co-variate for all models without introducing any internal variability (Wehner et al., 2020).

135 In this study, the GEV estimates are computed by introducing a linear co-variate into the
 136 location and the scale parameters while the shape parameter is fitted as constant in time (but not
 137 uniform across models and grid cells). In a warming world, all GEV parameters may vary between
 138 present-day and future climates, but a time-varying shape parameter would not be meaningful
 139 because of high estimate uncertainties due to the limited sampling. This assumption was advocated
 140 in recent related studies (e.g., (Cooley et al., 2007)) and widely used since then (Kharin et al.,
 141 2013; Wehner et al., 2020). In contrast, non-stationary location and scale parameters may further
 142 increase the quality of the fitted RX1DAY distribution in some regions. The cumulative distribution
 143 function for a non-stationary GEV distribution for a random variable X is:

$$F(x) = \exp \left\{ - \left[1 + \xi \frac{(x - \mu(t))}{\sigma(t)} \right]^{\frac{-1}{\xi}} \right\} \quad (1)$$

144

145 where the co-variate appears linearly in the GEV location parameter as $\mu(t) = \mu_0 + \mu_1 \log(CO_2)$
146 and in the scale parameter as $\sigma(t) = \sigma_0 + \sigma_1 \log(CO_2)$ while ξ is constant in time. This non-stationary
147 fit is performed for each grid point.

148 To reduce statistical uncertainty in fitting the GEV distributions, the entire RX1DAY time
149 series from 1850 to 2100 was used for all models. Having fitted GEV distribution, the precipitation
150 extremes of our interest are defined as the 20-year return values. Return values are calculated as
151 the exceedance of the annual extreme with probability p or as the quantiles of a GEV distribution.
152 The changes in the intensity of extreme events can be accordingly estimated for different future
153 periods or periods of different warming levels. Changes in the future (2051–2100) are computed
154 with respect to the historical period (1951–2014), while changes at different warming levels are
155 expressed relative to their intensity during the pre-industrial period (1850–1900).

156 2.3 Global warming levels

157 We frame the projections by considering the changes at a specified global warming target
158 of 1.5, 2 and 3 K above the pre-industrial level. Climate sensitivity, or the simulated global mean
159 surface air temperature response to more comprehensive radiative forcings, is different across differ-
160 ent models (Vial et al., 2013; Lee et al., 2021). As a consequence, the point in time when specified
161 global warming levels (GWLs) are achieved differs largely across models. Models with higher cli-
162 mate sensitivity reach specified GWLs earlier than others. However, some models may not even
163 reach the highest specified GWL before 2100. The first year when GWLs are reached for the 35
164 CMIP6 models used in this study under the scenario SSP5-8.5 is shown in the supplementary mate-
165 rial (Table S.1). The extreme precipitation statistics are then calculated for each model individually
166 over 21 years, extending from 10 years before and after the "central year". We have used a moving
167 average of 21 years before computing the central year.

168 2.4 Scaling of extreme precipitation with local and global temperature changes.

169 We scale changes in extreme precipitation (ΔRV_{20}) with both global mean surface air tem-
170 perature change ($\Delta GSAT$) and local surface air temperature change (ΔT). $\Delta GSAT$ is calculated as

171 the difference between the areal mean surface temperatures for the projected period and reference
 172 period (cf. Table S1). Similarly, ΔT is estimated as the local change in the climatological surface
 173 temperature or the rate of change of mean surface temperature at each grid point for the same
 174 periods as above. Instead of considering the linear rate of change ($R_{lin} = \Delta P_{ext}/\Delta T_{surf}$) of the
 175 extreme precipitation, we assume a multiplicative rate of change, i.e., $\Delta P_{ext} + 1 = (1 + R_{mul})^{\Delta T_{surf}}$.
 176 The multiplicative rate of change is thus calculated as:

$$R_{mul} = (\Delta P_{ext} + 1)^{\frac{1}{\Delta T_{surf}}} - 1, \quad (2)$$

177 where ΔP_{ext} is the change in precipitation extremes (here, $\Delta RV20$) and ΔT_{surf} is the change in
 178 surface temperature (either $\Delta GSAT$ or ΔT). Both the linear and the multiplicative rates become
 179 approximately equal ($R_{lin} \approx R_{mul}$) when $\Delta RV20 \ll 1$ mm/day. Another important point to note
 180 here is that for scaling with local temperature changes we masked the regions where the temperature
 181 changes are too small (i.e., $\Delta T \ll 1$ K) to avoid the infinite scaling while using equation (2). The
 182 masking is done only for those models which show $\Delta T \ll 1$ K, while we keep the others so that the
 183 results are calculated for the models which project a minimum surface warming.

184 2.5 Hypothesis testing

185 We also aim to identify the regions where the change in extreme precipitation may occur at
 186 a super-CC rate or sub-CC rate. In the latest IPCC report, (Seneviratne et al., 2021) conclude with
 187 high confidence that precipitation extremes are controlled by both thermodynamic and dynamic
 188 processes, and that warming-induced thermodynamic change results in an increase in extreme pre-
 189 cipitation at a rate that closely follows the CC relationship at the global scale. Any departure from
 190 the CC rate could therefore indicate an additional large-scale dynamical response. Attribution
 191 studies such as Pall et al. (2017) show the local dynamical responses lead to non-CC rates. Small
 192 scale dynamical responses such as enhanced convection, orographic lifting in atmospheric rivers, or
 193 wind intensification in tropical cyclones, can also induce a non-CC rate of change at the local scale.
 194 However, our analysis is only based on coarse resolution global CMIP6 models with parameterized
 195 convection so that the dynamical response here does not account for explicit mesoscale changes in
 196 the storm dynamics that could also modulate the extreme precipitation response (e.g. Chan et al.,

197 2020). Thus, the large scale dynamics are the only non-thermodynamic mechanisms that can be
 198 simulated by these models.

199 The blueprint we provide in section 4 will serve as a framework to an extended analysis on
 200 this matter. This can provide us with much confidence in the areas that are dominated by warming
 201 and those regions where changes in the circulation patterns may also matter. For this, we use
 202 a simple hypothesis test, where we identify the regions where, e.g., there is no change, using the
 203 80% confidence intervals we obtained from the multi-model framework. If the targeted R_{mul} (rate
 204 of change of RV20 with temperature) does not fall within the confidence interval calculated from
 205 the 35 models, we conclude that our hypothesis is rejected. When it comes in the range of the
 206 confidence interval, we accept the null hypothesis, and the regions are identified accordingly. To
 207 identify the regions with no change, we consider the null-hypothesis $R_{mul} = 0\%/C$, while $R_{mul} =$
 208 $7\%/K$ is used as our second hypothesis to find regions of sub-, super-, or consistent with the CC
 209 rate.

210 3 Results

211 3.1 Intensification of extreme precipitation

212 Figure 1 shows the analysis for the median, 10th, and 90th percentiles along with the un-
 213 certainty range, which is, the difference between the 90th and 10th percentiles, of the extreme
 214 precipitation changes scaled by both the global mean ($\Delta GSAT$, left panel) and local mean (ΔT ,
 215 right panel) surface air temperature changes. The extreme precipitation rate as a function of both
 216 $\Delta GSAT$ and ΔT shows a clear increase in its intensity with respect to the historical period (1951-
 217 2014). The global average of the multi-model median changes is $5.0\%/K$ (Figure 1 c) for the scaling
 218 with $\Delta GSAT$, while it is $5.3\%/K$ (Figure 1 d) for that of ΔT . These close values are slightly smaller
 219 than the CC rate of $\approx 7\%/K$, which suggests some negative dynamical influence at the regional
 220 scale in increasingly subsiding regions, but also some water limitation in such dry regions.

221 From the maps in figure 1 c, d, the overall large-scale patterns of change remain similar for
 222 both temperature scalings, although changes are a bit more pronounced for the scaling with local
 223 temperatures. The largest percentage of increase occurs over the tropical areas followed by the

224 high latitudes for the global temperature scaling. For the local scaling, the largest percentage of
225 changes occurs over the tropics followed by the mid-latitude oceans. The stronger warming over
226 the continental landmass can be a major reason for these differences (Wang et al., 2017). Certain
227 regions over the ocean like the north Atlantic and the southern oceans in figure 1c are characterized
228 by moderate to high scaled changes in precipitation extremes, which can be linked to the limited
229 changes in the projected local surface temperatures.

230 Changes in extreme precipitation with Δ GSAT and Δ T scalings vary substantially across
231 the globe. Over most of the mid-latitude land areas, changes do not strongly depend on the scaling
232 method and exhibit a sub-CC rate of 0–4%/K. Over the subtropics, the assessed rate of change
233 deviates further from the CC rate. In particular, there are high rates (super CC) over the Sahara
234 and the intertropical convergence zone (ITCZ), while the climatological dry areas like the basins
235 of the South Pacific, the north and the south Atlantic, and the south Indian Ocean are marked
236 by reduced, or even negative, rates of change in the extremes. Again, this deviation from the
237 CC rate ($\approx 7\%/K$) indicates some other factors apart from the thermodynamic features might be
238 at play. Notably, a remarkable property is the increased multi-model spread over these regions
239 (ref., supplementary material), in line with the less robust dynamical response across global climate
240 models (Pfahl et al., 2017). Large departures, whether it is positive or negative, from the CC rate
241 are associated with a larger inter-model spread, suggesting that these regions may be influenced
242 by less robust changes in atmospheric circulation, possibly related to model-dependent patterns of
243 sea surface temperature anomalies or land-sea temperature contrasts (Douville and John, 2021).
244 Another noticeable feature is the impact of the scaling method over the northern high-latitudes.
245 This is partly linked to the Arctic amplification, where the Arctic region gets warm more than twice
246 as fast as the global average (Cohen et al., 2014).

247 **3.2 Range of projected responses in extreme precipitation**

248 Figure 1 a, b, e and f illustrate the 10th and 90th percentiles of extreme precipitation rates
249 for scalings with with global and local warming. The lower and the upper tails of distribution help
250 us to study the worst possible case scenarios and more importantly quantify the uncertainties. The
251 lower tails of extreme precipitation rates are characterized by large-scale features like the negative

252 scaling over the subtropical oceans in the western continental boundaries for both global and local
253 temperature scaling. It is important to note that these regions are predominantly dry areas due
254 to the descending branches of the Hadley cells. The rest of the globe is marked by very small
255 changes either positive or negative that are very close to zero. However, the 90th percentile maps
256 or the upper tail of the distribution show a strong positive increase in precipitation extremes almost
257 everywhere around the globe. These are consistent with super-CC rates (stippling) for the scaling
258 with global warming and, to a large extent, with local warming. Typical to the local warming
259 scaling, the northern mid- and high-latitude land areas are not stippled. This means that the rate
260 of change in extreme precipitation with local warming is sub-CC over these regions even for the
261 90% quantiles. Moreover, this is consistent across the three maps in the right panel of Figure 1 b,
262 d, f. This results directly from a larger and consistent local warming over these areas, especially in
263 the Arctic.

264 Another noticeable result is the zero or low-density stippling over the tropical Atlantic ocean,
265 Southern Europe, Chilean Coast, Continental North America and South Africa in all maps of both
266 global and local temperature scalings (figure 1). This implies a sub-CC rate over these areas
267 irrespective of the scaling choice. We speculate that the circulation changes, such as a broadening
268 of the subtropical subsidence region, might be responsible for this (Pfahl et al., 2017). Indeed
269 this kind of extension can effectively replace a low-level moisture convergence zone with a regime
270 with low-level divergence where there is a weaker connection between the projected changes in
271 precipitable water versus temperature.

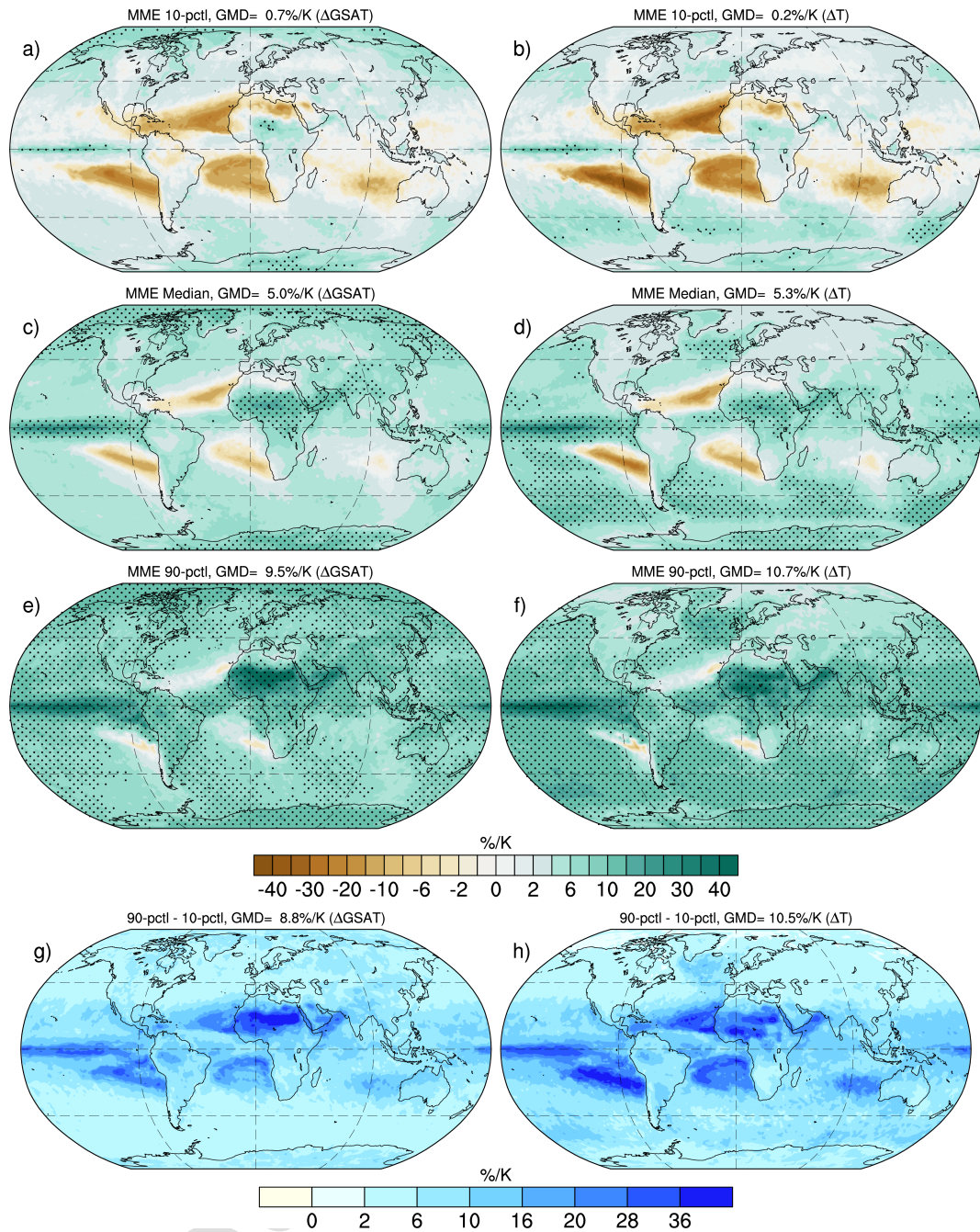


Figure 1: Projected relative changes (%/K) in 20-yr return values of RX1DAY scaled by both global mean surface temperature change ($\Delta GSAT$ in K, left panel) and local mean surface temperature change (ΔT in K, right panel). The changes are calculated for the future period of 2051-2100 relative to the historical period of 1951-2014 using the SSP5-8.8 scenario. (a),(b) show the 10% quantile maps, (c),(d) shows the median maps and (e),(f) show the 90% quantile maps, calculated from the CMIP6 multimodel ensemble. The bottom panel shows the width of the confidence range of extreme precipitation, computed as the difference between the 90% and 10% quantile maps. Stippling highlights the grid cells where the rate of change is more than 7%/K for respective scalings with $\Delta GSAT$ (left panel) and ΔT (right panel). GMD denotes the global mean differences.

272 The bottom panels (g, h) in figure 1 show the difference between the 10th and 90th percentile
273 values as simulated by a single realization from 35 CMIP6 models. Large differences between the
274 upper and lower quantiles indicate a substantial spread in the projected extreme precipitation
275 changes. These maps quantify the uncertainties in extreme precipitation response and the pattern
276 is very similar to those of the inter-model standard deviation maps as stated earlier in section 3.1
277 (also ref., supplementary material). As clearly depicted in these figures, the spread is larger over
278 tropical areas than the rest of the globe. Particularly, over the tropics, the values are notably large
279 in the regions which are climatologically dry or wet, e.g., the subsidence zones of the Hadley cells,
280 the ITCZ, and the Saharan desert. We also see that the overall pattern of the inter-model spread is
281 similar for both temperature scalings. Table 1 reflects the range of model uncertainty in projected
282 changes in extreme precipitation with respect to both local as well as global warming. It summarizes
283 the areal averages of the median, 10%-, 90%- quantiles and their difference for the total (global)
284 area, the global land, and global ocean areas separately. It is clear from this Table that the width of
285 confidence range averaged globally is large, about 10.5%, which is more than the average CC rate.

286 Several sources of uncertainty can contribute to this spread. The main source is likely due
287 to different representations of the relevant physical processes and to related biases in the models'
288 climatology of present-day precipitation. Moreover, the non-homogeneous temperature gradient
289 from the equator to the poles and the land/sea temperature differences is also a source of larger
290 uncertainty in the local temperature scaling maps. Another potential source of uncertainty is the
291 internal climate variability which also gets translated differently into the total uncertainty with the
292 use of different temperatures for scaling. We discuss potential contribution of internal variability in
293 the next section.

| | | 10 | med | 90 | width (90-10) | |
|--------------|------|---------|------|-----|---------------|-------------|
| Total | GSAT | CMIP6 | 0.7 | 5.0 | 9.5 | 8.8 |
| | | CanESM5 | 3.3 | 4.8 | 6.2 | 2.9 |
| | T | CMIP6 | 0.2 | 5.3 | 10.7 | 10.5 |
| | | CanESM5 | 3.2 | 5.0 | 6.8 | 3.6 |
| Land | GSAT | CMIP6 | 1.5 | 5.8 | 11.1 | 9.5 |
| | | CanESM5 | 4.3 | 5.9 | 7.4 | 3.1 |
| | T | CMIP6 | 1.0 | 4.6 | 9.3 | 8.3 |
| | | CanESM5 | 3.4 | 4.7 | 6.0 | 2.5 |
| Ocean | GSAT | CMIP6 | 0.3 | 4.6 | 8.8 | 8.5 |
| | | CanESM5 | 2.9 | 4.3 | 5.7 | 2.8 |
| | T | CMIP6 | -0.1 | 5.6 | 11.4 | 11.5 |
| | | CanESM5 | 3.1 | 5.1 | 7.1 | 4.0 |

Table 1: Areal mean values (in %/K) of 10%-, 90%- quantiles and median of the extreme precipitation changes scaled by both Δ GSAT and Δ T over the total global area, global land, and global oceans. The table includes the respective values for both the CMIP6 multi-model changes and CanESM5 multi-ensemble changes.

294 3.3 Role of internal variability

295 The spread among the single realizations of CMIP6 projections has been mainly interpreted
296 so far as model uncertainty. Yet, it can also arise from internal variability given the limited sam-
297 pling. In the case of historical extreme precipitation changes at a multi-decadal time scale, internal
298 variability was shown to be a significant driver due to the cancellation between different external
299 forcings (Nath et al., 2018). To get more insight into this, we analyzed the rate of change in precip-
300 itation extremes in the 25-member ensemble of the CanESM5 model, and assess the spread across
301 members (figure 2). We consider the large ensemble from CanESM5 as a representative estimate of
302 the internal variability range. It should be noted that CanESM5 is one of the low-resolution CMIP6
303 models, with moderate skill in simulating global extreme precipitation (Wehner et al., 2020). It
304 is also one of the CMIP6 models with the highest climate sensitivity, but this effect is accounted
305 for by the scaling. The globally averaged median values are thus very close between the CMIP6
306 ensemble and the CanESM5 ensemble for both scaling with ΔGSAT and ΔT (Table 1).

307 Figure 2 shows the same diagnostics as in figure 1, but we see an obvious visible difference
308 between them along with a few matching large scale patterns. For instance, the rates of change
309 for both ΔGSAT and ΔT match over the climatologically dry regions like the north and south
310 tropical Atlantic oceans as well as over primarily wet regions like the inter-tropical convergence
311 zone. Furthermore, the regions like North American inland, Europe and Eurasia, Chilean Coasts,
312 and South Africa are marked by a sub-CC rate of change with both temperature scales, likewise in
313 figure 1. Another noticeable result here is the changes in the areas that are stippled. CanESM5
314 shows areas of super-CC ($>7\%/K$) even for the 10th percentile maps which are not observed in
315 the CMIP6 ensemble. While for 90th percentile maps we see a decrease in the regions that are
316 super-CC rated. The range of uncertainties ($2.9\%/K$ for ΔGSAT and $3.6\%/K$ for ΔT) across the
317 CanESM5 ensemble members is evidently less than that across the CMIP6 models. The total
318 uncertainties depicted in Figure 2 (bottom panel) is just the result of internal variability. Table 1
319 again summarizes the mean value of median, 10%-, 90%- quantiles and their difference for the total
320 (global) area, the global land, and global ocean areas separately.

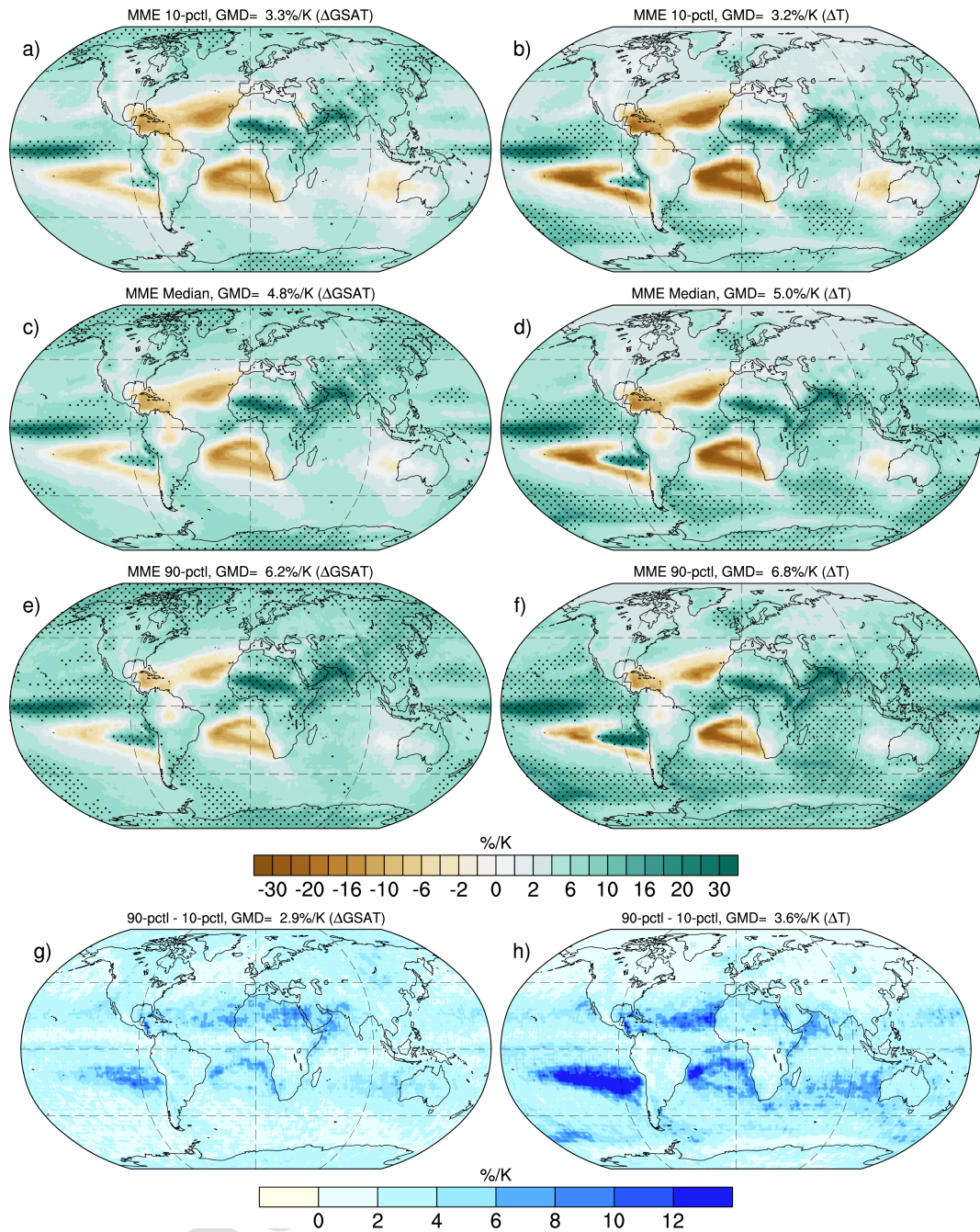


Figure 2: Same as figure 1, but for the ensemble of 25 individual members of CanESM5 model.

321 The evidenced range of uncertainty for the large ensemble of CanESM5 suggests that internal
 322 variability can contribute significantly to the total uncertainty of extreme precipitation rates, when
 323 estimated from one single simulation, even in a very high emission scenario. Figure 3 depicts the

324 ratio of the width of the confidence range (the difference between 90% and 10% quantiles) of the
 325 CanESM5 large ensemble to that of the CMIP6 cross model ensemble. We clearly see that for mean
 326 extreme precipitation rates scaled by global mean surface temperature, internal variability alone
 327 can induce a range of response about half as large as the CMIP6 multi-model spread (global average
 328 of $\approx 40\%$). For the high- and mid-latitude regions, internal variability is even larger and explains
 329 a range of response $\approx 75\%$ (darker shades of blue) as large as the total uncertainty. These regions
 330 exhibit a low to moderate increase in the percentage response of the extreme precipitation (as shown
 331 in figures 1, 2) which explains the strong influence that internal variability may have on the extreme
 332 precipitation signals. However, throughout the equatorial belt and the adjacent tropical areas, we
 333 see a rather less but non-negligible contribution from internal variability. Interestingly, most of
 334 these regions fall along with the average position of the ITCZ, which is characterized by high values
 335 of extreme precipitation changes. Here, model uncertainty is very likely the major contributor to
 336 the assessed inter-model spread, whereas internal variability only contributes to about 0–20% but
 337 is still potentially significant.

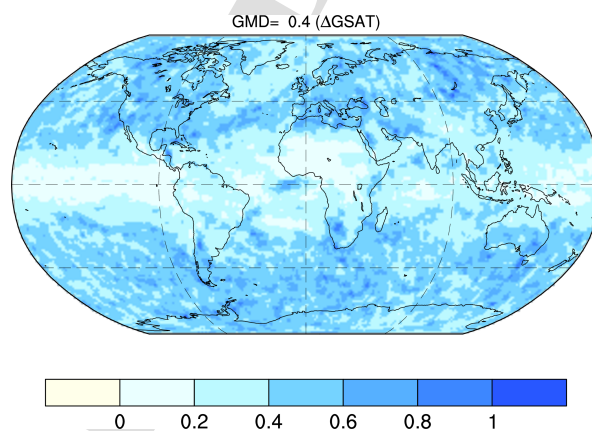


Figure 3: Ratio of the width of confidence range of extreme precipitation in large ensemble CanESM5 to the CMIP6 multi-model ensemble. The result shown here is for scaling with global mean surface temperature change ($\Delta GSAT$).

338 Overall, these results suggest that internal variability contributes substantially to the assessed
 339 uncertainty (i.e., the width of the 80% confidence range) reported in Figure 1. As a consequence,
 340 modeling uncertainty alone is probably less than shown in Figure 1. Filtering out internal variability
 341 could be done by using multiple members for each CMIP6 model involved — but such data are not

342 available for all models so far.

343 3.4 Sensitivity of precipitation extremes at different global warming levels

344 Figure 4 provides analyses of the 10%- and 90%- quantiles of global climate sensitivity of
345 RV20 in the CMIP6 ensembles at GWLs of 1.5 K, 2 K, and 3 K respectively. The median changes
346 (figure not shown) relative to the preindustrial period for all GWLs are close to the CC rate of
347 $\approx 7\%/K$. Not surprisingly, globally these scaled rates of change in precipitation do not appear to
348 depend on the selected GWL. There is only a slight difference of $0.7\%/K$ in the average multi-model
349 median as the GWL is increased from 1.5K to 3 K possibly due to a non-linear response in some
350 models (e.g., Pendergrass et al. (2019) based on a CMIP5 model), or just a sampling uncertainty.
351 A notable observation as summarized in Table 2 is that the inter-model uncertainty range tends to
352 decrease as the GWL increases. The lower-tail of the extreme precipitation rates shown by 10th
353 percentile maps for the three GWLs (figure 4 left panel) reveals a very small decrease in the average
354 negative precipitation rate values from $1.2\%/K$ (+1.5K) to $1.1\%/K$ (+2K) and to $1.0\%/K$ (+3K).
355 Also, as seen from the right panel of Figure 4, the upper-tail of the distribution or the 90th per-
356 centile maps show that the upper bound of extreme precipitation rates move closer to the median
357 value from $14.9\%/K$ (+1.5K) to $13.6\%/K$ (2K) and $12.1\%/K$ (3K). This reduced uncertainty for
358 higher GWLs is consistent with the expected contribution of internal variability. At lower GWLs,
359 the forced response remains limited, and the additional noise resulting from internal variability is
360 proportionally larger. This finding provides support for investigating changes in extreme precip-
361 itation at high GWLs. Moreover, we notice that the uncertainty at +3K GWL remains larger
362 than that reported in Figure 1. Again, this is consistent with a smaller contribution of internal
363 variability in Figure 1 compared to a +3K GWL — consistent with the fact that SSP5-8.5 leads
364 to global warming higher than +3K in most CMIP6 models, and that estimating changes over a
365 longer period (50-yr in Fig 1, vs 20-yr for GWLs) leads to better filtering of internal variability.

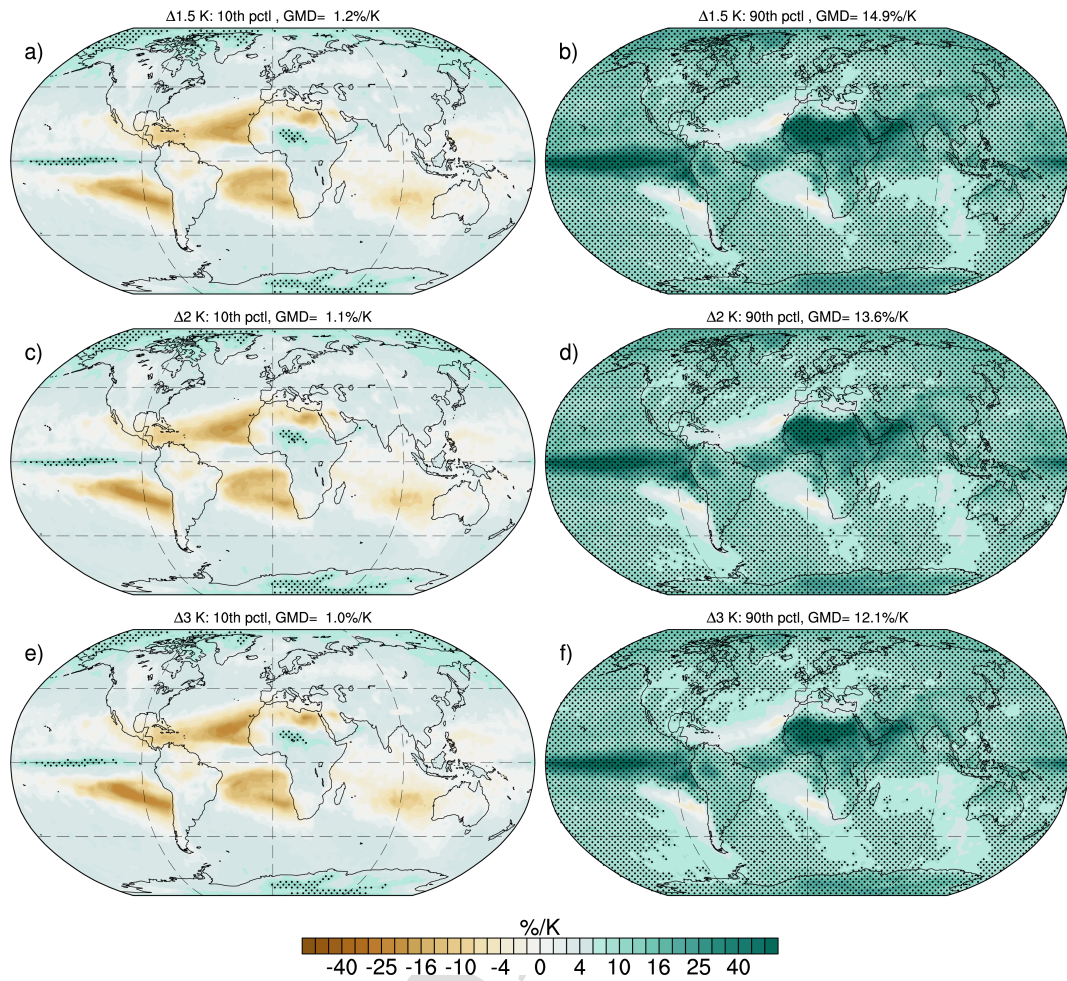


Figure 4: Projected relative changes (%/K) in 20-yr return values of RX1DAY scaled by global mean surface temperature change (Δ GSAT in $^{\circ}$ K) at global warming levels of 1.5, 2 and 3 $^{\circ}$ K above the preindustrial (1850-1900) average values. The left panel shows the 10% quantile maps and the right panel shows 90% quantile maps for the CMIP6 multimodel changes. Stippling marks the grid cells where the rate of change is more than 7%/K. GMD denotes the global mean differences.

| | | 10 | med | 90 | width (90-10) |
|--------------|------|-----|-----|------|---------------|
| Total | 1.5K | 1.2 | 6.5 | 14.9 | 13.7 |
| | 2K | 1.1 | 6.2 | 13.6 | 12.5 |
| | 3K | 1.0 | 5.9 | 12.0 | 11.0 |
| Land | 1.5K | 2.0 | 7.5 | 19.3 | 17.4 |
| | 2K | 1.9 | 7.2 | 17.3 | 15.4 |
| | 3K | 1.8 | 6.8 | 14.8 | 13.0 |
| Ocean | 1.5K | 0.8 | 6.0 | 12.9 | 12.1 |
| | 2K | 0.8 | 5.8 | 12.0 | 11.2 |
| | 3K | 0.6 | 5.4 | 10.8 | 10.2 |

Table 2: Areal mean values (in %/K) of 10%- and 90%- quantiles of the extreme precipitation changes scaled by $\Delta GSAT$ over the total global area, global land, and global oceans for three target global warming levels of 1.5, 2, and 3 °K.

3.5 Regions of hypothesis tests

Using a simple hypothesis test as described in Section 2.5, we classified the global areas into three categories. Here we have considered two general hypotheses — (H_0) extreme precipitation does not change with global warming, and (H_1, H_2) the change in extreme precipitation follows the CC rate of $\approx 7\%/K$ for $\Delta GSAT$ and ΔT scaling, respectively. Figure 5 shows the regions categorized accordingly to our hypotheses. Red and blue colors are regions where the hypothesis is rejected while yellow represents regions where the hypothesis is accepted. It is important to notice that accepting a hypothesis doesn't mean that this hypothesis is true. It rather means that the

374 hypothesis is plausible, i.e., there is not enough evidence to reject it.

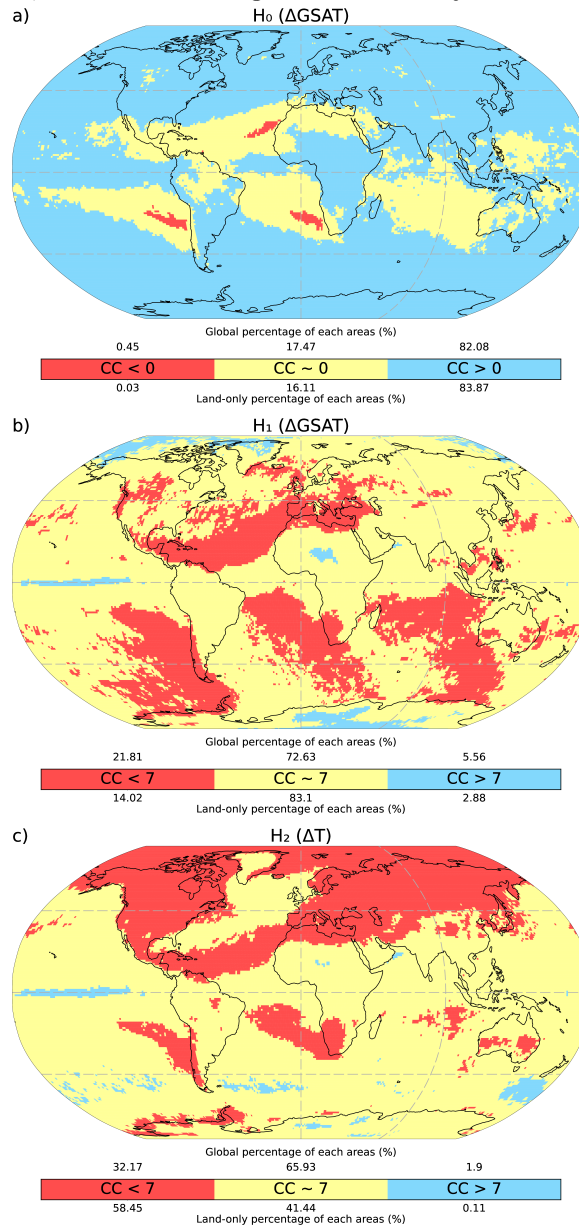


Figure 5: Global maps of confidence areas (80% confidence interval) for the CMIP6 using 35 individual models with a single realization. The maps show where the rate of extreme precipitation changes is consistent with constant rates of $\approx 0\%/K$ or $\approx 7\%/K$. Red color denotes the regions where the changes are always less than the constant, yellow denotes areas where the constant falls within the confidence interval and blue denotes areas where the rates are always greater than the constant. Map (a) shows the areas where the rate of changes in extreme precipitation remains unchanged or consistent to $0\%/K$ when scaled with $\Delta GSAT$. Maps (b), (c) show the global areas where the rate of changes are consistent with the CC rate of $\approx 7\%/K$ with respect to $\Delta GSAT$ and ΔT . The values on top of colorbar show the percentage of each colored area over the global land surface, while the values at the bottom indicate the same over the total global surface.

375 Figure 5 a shows the regions all over the globe where the rate of precipitation change to
 376 ΔGSAT is consistent with $\approx 0\%/K$ (i.e., no significant change, yellow color). We see that the
 377 regions for which H_0 cannot be rejected are limited and these are especially over the global oceans.
 378 It is to be noted that over these regions the median values of the projected precipitation changes
 379 are consistently low and close to zero. The same results are found for the local temperature scaling
 380 (with a correlation $\approx 99\%$). Over these regions, the cohort of CMIP6 models does not provide robust
 381 evidence that global warming will intensify extreme precipitation. While the small patches of red
 382 colored regions over subtropical ocean west to the continents indicate that the hypothesis is rejected
 383 but the changes are negative. Another notable feature over the yellow and red colored regions is
 384 the similarity of negative scaling the figure 5a to the patterns of negative dynamic contribution
 385 as observed in figure 3 of Pfahl et al. (2017) for the CMIP5 models. This implies a consistency
 386 between the CMIP5 and CMIP6 projections of extreme precipitation, possibly for a common reason,
 387 perhaps, a less robust dynamical response. The negative dynamic factors may perchance responsible
 388 for keeping the extreme precipitation not to increase at large as it does with moisture increase in
 389 the rest of the globe. Remarkably, there is no land region where extreme precipitation is robustly
 390 expected to decrease in response to global warming.

391 Figure 5 b, c shows the regions where the hypotheses H_1 , H_2 are accepted or rejected.
 392 Both H_1 and H_2 are used for identifying the regions where the extreme precipitation changes are
 393 consistent with the CC rate of $\approx 7\%/K$ with respect to ΔGSAT and ΔT respectively. These maps
 394 can be used as a blueprint to identify the regions which are consistent with the CC rate and those
 395 which are not. The first outcome is that a vast majority of places on Earth, about 83% of the global
 396 land area, are expected to undergo a change in extreme precipitation that is consistent with the CC
 397 rate, particularly with the ΔGSAT scaling. This doesn't mean that these regions will experience a
 398 change of exactly $+7\%/K$. It means that, over these regions, the expected change in RX1d is not
 399 robustly sub-CC or super-CC, i.e., not inconsistent with CC. The majority of regions that follow a
 400 sub-CC rate of change for both temperature scalings are over the oceans, especially at the western
 401 continental boundaries, which are climatologically dry regions. A few continental regions like the
 402 North American continent, South and Central Eastern Europe, Chilean Coast, South Africa and

403 South Australia are also marked by the sub-CC rate for both scaling temperatures. There are also
404 patches of consistent super-CC rates over the equatorial Pacific and the Sahel region. Scaling with
405 two different temperatures displays different areas of consistency with CC especially over the high
406 Northern latitudes. The map for the local temperature scaling shows a significant increase in the
407 sub-CC areas especially over the Arctic and most of the mid-latitude landmasses. This indicates
408 that the expected increase in extreme precipitation over these regions does not follow the local
409 warming at the CC rate. This result is consistent with the enhanced warming expected over these
410 regions, while the surrounding oceans (the main source of moisture) are warming less quickly.

411 **4 Discussion and conclusion**

412 Despite an overall agreement that extreme precipitation follow a $\approx 7\%/K$ rate of increase
413 at the global scale, projected changes in extreme precipitation are influenced by multiple factors
414 that can lead to large uncertainties at the regional scale. In this study, we quantify uncertainty in
415 the projected changes in extreme precipitation — while most studies look at the mean or median
416 change across an ensemble of models — using a single high-emission scenario. We provide a first
417 assessment of the 10-90% range in the extreme daily precipitation responses at the grid-point scale
418 and a global picture of the regions where changes in extreme precipitation are consistent with the
419 CC rate. Our results suggest that uncertainty is usually quite large. Averaged globally, GSAT
420 scaling ranges extend from about 0 up to a super-CC rate, with a median close to the CC rate.
421 Uncertainty can be larger if changes in extreme precipitation are investigated for a given GWL.
422 This may be an artifact of internal variability due to the lack of sampling which has a stronger
423 relative contribution at lower GWLs compared to our selected very-high emissions scenario.

424 Our assessed CMIP6 uncertainty arises both from model uncertainty and internal variability,
425 as our calculations are based on single runs from each CMIP6 model. Internal variability can be seen
426 as a basic sampling uncertainty, which could be overcome by averaging across multiple members
427 for each global climate model. Model uncertainty alone would lead to narrower ranges than those
428 reported in this study. However, despite the widening induced by a non-negligible contribution of
429 internal variability, our results show that the intensification of extreme daily precipitation is robust
430 over most regions, with more than 90% of models simulating an increase of 20-yr RVs. We believe

431 that this study helps strengthen our confidence in the intensification of extreme precipitation.

432 Most regions around the world exhibit a RV20 change consistent with the CC rate of $\approx 7\%/K$.
433 Remarkably, about 83% of the global land fraction is consistent with this rate of change when scaled
434 by $\Delta GSAT$. Exceptions to this include limited areas over subtropical oceans (showing a signifi-
435 cantly sub-CC rate), and parts of the equatorial Pacific and Sahelian ITCZ (showing a significantly
436 super-CC rate). These findings are consistent with well-known projected changes in large-scale
437 atmospheric circulation, i.e., strengthened subsidence over the subtropics and enhanced convection
438 over the core of the ITCZ (Douville et al., 2021). Not surprisingly, the rate of change in the Arctic
439 is particularly sensitive to the scaling applied, since this region is warming much faster than the
440 global average. This example suggests that the spatial distribution of the warming (e.g., Arctic
441 amplification, land-sea contrast) can be also responsible for changes in the low-level atmospheric
442 circulation and, therefore, for the departure from the CC rate of intensification.

443 Due to the uncertainty, the rate of change in extreme precipitation depicted here only repre-
444 sents a plausible scenario. This hints at the fact that we cannot produce a more accurate projection
445 until we limit both model uncertainty and internal variability. Better filtering of internal variability
446 would require using multiple ensemble members for each CMIP model — which are not available at
447 the moment except for a few models. Therefore, we suggest to the modeling community to consider
448 producing a minimum number (at least 9 according to O'Neill et al. (2016)) of realizations for
449 each selected emissions scenario in the forthcoming CMIP7 exercise. Beyond internal variability,
450 evidence suggests that modeling uncertainty also contributes to a large fraction of the reported
451 uncertainty. This source of uncertainty is related to our limited knowledge of the key physical
452 processes controlling the response of extreme precipitation that is simulated by both global and
453 regional climate models. Thus the generation of large ensembles along with other improvements
454 like the development and wider use of convection-permitting models (Lucas-Picher et al., 2021)
455 could increase the reliability of projected changes in extreme precipitation. Other methods such as
456 the development and application of observational constraints (Ribes et al., 2021) could be also very
457 useful to constrain the response of both global and regional climate models.

458 Declaration of competing interest

459 The authors declare that they have no known competing financial interests or personal
460 relationships that could have appeared to influence the work reported in this paper.

461 Acknowledgements

462 This work is part of the Climate Advanced Forecasting of sub-seasonal Extremes (CAFE)
463 project, which has received funding from the European Union's Horizon 2020 research and inno-
464 vation program under the Marie Marie Sklodowska-Curie grant agreement No 813844. We ac-
465 knowledge the World Climate Research Programme's Working Group on Coupled Modelling, which
466 is responsible for CMIP, and we thank the climate modeling groups for producing and making
467 available their model output to CMIP. We also thank the Institut Pierre-Simon Laplace (ISPL)
468 Mésocentre for Climate Sciences for the CMIP6 data acquisition, storage space, and intensive com-
469 puting resources for this paper.

470 **References**

- 471 L. V. Alexander, X. Zhang, T. C. Peterson, J. Caesar, B. Gleason, A. Klein Tank, M. Haylock,
472 D. Collins, B. Trewin, F. Rahimzadeh, et al. Global observed changes in daily climate extremes
473 of temperature and precipitation. *Journal of Geophysical Research: Atmospheres*, 111(D5), 2006.
- 474 R. P. Allan and B. J. Soden. Atmospheric warming and the amplification of precipitation extremes.
475 *Science*, 321(5895):1481–1484, 2008.
- 476 M. R. Allen and W. J. Ingram. Constraints on future changes in climate and the hydrologic cycle.
477 *Nature*, 419(6903):228–232, 2002.
- 478 S. Arrhenius. Xxxi. on the influence of carbonic acid in the air upon the temperature of the ground.
479 *The London, Edinburgh, and Dublin Philosophical Magazine and Journal of Science*, 41(251):
480 237–276, 1896.
- 481 B. Asadieh and N. Y. Krakauer. Global trends in extreme precipitation: climate models versus
482 observations. *Hydrology and Earth System Sciences*, 19(2):877–891, 2015.
- 483 M. Bador, M. G. Donat, O. Geoffroy, and L. V. Alexander. Assessing the robustness of future
484 extreme precipitation intensification in the cmip5 ensemble. *Journal of Climate*, 31(16):6505–
485 6525, 2018.
- 486 P. Berg, J. Haerter, P. Thejll, C. Piani, S. Hagemann, and J. Christensen. Seasonal characteristics
487 of the relationship between daily precipitation intensity and surface temperature. *Journal of*
488 *Geophysical Research: Atmospheres*, 114(D18), 2009.
- 489 S. C. Chan, E. J. Kendon, S. Berthou, G. Fossier, E. Lewis, and H. J. Fowler. Europe-wide precipi-
490 tation projections at convection permitting scale with the unified model. *Climate Dynamics*, 55
491 (3):409–428, 2020.
- 492 J. Cohen, J. Screen, J. Furtado, M. Barlow, D. Whittleston, D. Coumou, J. Francis, K. Dethloff,
493 D. Entekhabi, J. Overland, et al. Recent arctic amplification and extreme mid-latitude weather,
494 *nat. geosci.*, 7, 627–637, 2014.

- 495 S. Coles, J. Bawa, L. Trenner, and P. Dorazio. *An introduction to statistical modeling of extreme*
496 *values*, volume 208. Springer, 2001.
- 497 D. Cooley, D. Nychka, and P. Naveau. Bayesian spatial modeling of extreme precipitation return
498 levels. *Journal of the American Statistical Association*, 102(479):824–840, 2007.
- 499 H. Douville and A. John. Fast adjustment versus slow sst-mediated response of daily precipitation
500 statistics to abrupt 4xco 2. *Climate Dynamics*, 56(3):1083–1104, 2021.
- 501 H. Douville, K. Raghavan, J. Renwick, R. Allan, P. Arias, M. Barlow, R. Cerezo-Mota, A. Cherchi,
502 T. Gan, J. Gergis, D. Jiang, A. Khan, W. Pokam Mba, D. Rosenfeld, J. Tierney, and O. Zolina.
503 Water cycle changes. In Masson-Delmotte, V., P. Zhai, A. Pirani, S. L. Connors, C. Péan,
504 S. Berger, N. Caud, Y. Chen, L. Goldfarb, M. I. Gomis, M. Huang, K. Leitzell, E. Lonnoy,
505 J. B. R. Matthews, T. K. Maycock, T. Waterfield, O. Yelekçi, R. Yu, and B. Zhou, editors,
506 *Climate Change 2021: The Physical Science Basis. Contribution of Working Group I to the Sixth*
507 *Assessment Report of the Intergovernmental Panel on Climate Change*, chapter 11. Cambridge
508 University Press. In Press., 2021.
- 509 D. R. Easterling, K. E. Kunkel, M. F. Wehner, and L. Sun. Detection and attribution of climate
510 extremes in the observed record. *Weather and Climate Extremes*, 11:17–27, 2016.
- 511 V. Eyring, S. Bony, G. A. Meehl, C. A. Senior, B. Stevens, R. J. Stouffer, and K. E. Taylor.
512 Overview of the coupled model intercomparison project phase 6 (cmip6) experimental design and
513 organization. *Geoscientific Model Development*, 9(5):1937–1958, 2016.
- 514 R. Hardwick Jones, S. Westra, and A. Sharma. Observed relationships between extreme sub-daily
515 precipitation, surface temperature, and relative humidity. *Geophysical Research Letters*, 37(22),
516 2010.
- 517 S.-C. Kao and A. R. Ganguly. Intensity, duration, and frequency of precipitation extremes under
518 21st-century warming scenarios. *Journal of Geophysical Research: Atmospheres*, 116(D16), 2011.
- 519 T. R. Karl and D. R. Easterling. Climate extremes: Selected review and future research directions.
520 *Climatic change*, 42(1):309–325, 1999.

- 521 T. R. Karl, N. Nicholls, and A. Ghazi. Clivar/gcos/wmo workshop on indices and indicators for
522 climate extremes workshop summary. In *Weather and climate extremes*, pages 3–7. Springer,
523 1999.
- 524 V. V. Kharin, F. W. Zwiers, X. Zhang, and G. C. Hegerl. Changes in temperature and precipitation
525 extremes in the ipcc ensemble of global coupled model simulations. *Journal of Climate*, 20(8):
526 1419–1444, 2007.
- 527 V. V. Kharin, F. Zwiers, X. Zhang, and M. Wehner. Changes in temperature and precipitation
528 extremes in the cmip5 ensemble. *Climatic change*, 119(2):345–357, 2013.
- 529 R. Knutti and D. Masson. D. & a. gettelman (2013). *Climate Model Genealogy: Generation CMIP5*
530 *and How we got there*, pages 1194–1199, 2013.
- 531 J. Lee, J. Marotzke, G. Bala, L. Cao, S. Corti, J. Dunne, F. Engelbrecht, E. Fischer, J. Fyfe,
532 C. Jones, et al. Future global climate: scenariobased projections and near-term information.
533 *Climate change*, 2021.
- 534 F. Lehner, C. Deser, N. Maher, J. Marotzke, E. M. Fischer, L. Brunner, R. Knutti, and E. Hawkins.
535 Partitioning climate projection uncertainty with multiple large ensembles and cmip5/6. *Earth*
536 *System Dynamics*, 11(2):491–508, 2020.
- 537 C. Li, F. Zwiers, X. Zhang, G. Li, Y. Sun, and M. Wehner. Changes in annual extremes of daily
538 temperature and precipitation in cmip6 models. *Journal of Climate*, pages 1–61, 2020.
- 539 P. Lucas-Picher, D. Argüeso, E. Brisson, Y. Trambly, P. Berg, A. Lemonsu, S. Kotlarski, and
540 C. Caillaud. Convection-permitting modeling with regional climate models: Latest developments
541 and next steps. *Wiley Interdisciplinary Reviews: Climate Change*, page e731, 2021.
- 542 Masson-Delmotte, V., P. Zhai, A. Pirani, S. L. Connors, C. Péan, S. Berger, N. Caud, Y. Chen,
543 L. Goldfarb, M. I. Gomis, M. Huang, K. Leitzell, E. Lonnoy, J. B. R. Matthews, T. K. Maycock,
544 T. Waterfield, O. Yelekçi, R. Yu, B. Zhou, and (eds.). Ipcc, 2021: Summary for policymakers. In
545 *Climate Change 2021: The Physical Science Basis. Contribution of Working Group I to the Sixth*

- 546 *Assessment Report of the Intergovernmental Panel on Climate Change*. Cambridge University
547 Press. In Press., 2021.
- 548 S.-K. Min, X. Zhang, F. W. Zwiers, and G. C. Hegerl. Human contribution to more-intense precip-
549 itation extremes. *Nature*, 470(7334):378–381, 2011.
- 550 R. Mizuta and H. Endo. Projected changes in extreme precipitation in a 60-km agcm large ensemble
551 and their dependence on return periods. *Geophysical Research Letters*, 47(13):e2019GL086855,
552 2020.
- 553 C. J. Muller, P. A. O’Gorman, and L. E. Back. Intensification of precipitation extremes with
554 warming in a cloud-resolving model. *Journal of Climate*, 24(11):2784–2800, 2011.
- 555 R. Nath, Y. Luo, W. Chen, and X. Cui. On the contribution of internal variability and external
556 forcing factors to the cooling trend over the humid subtropical indo-gangetic plain in india.
557 *Scientific reports*, 8(1):1–11, 2018.
- 558 B. C. O’Neill, C. Tebaldi, D. P. v. Vuuren, V. Eyring, P. Friedlingstein, G. Hurtt, R. Knutti,
559 E. Kriegler, J.-F. Lamarque, J. Lowe, et al. The scenario model intercomparison project (scenar-
560 iomip) for cmip6. *Geoscientific Model Development*, 9(9):3461–3482, 2016.
- 561 P. A. O’Gorman. Precipitation extremes under climate change. *Current climate change reports*, 1
562 (2):49–59, 2015.
- 563 P. Pall, M. Allen, and D. A. Stone. Testing the clausius–clapeyron constraint on changes in extreme
564 precipitation under co 2 warming. *Climate Dynamics*, 28(4):351–363, 2007.
- 565 P. Pall, C. M. Patricola, M. F. Wehner, D. A. Stone, C. J. Paciorek, and W. D. Collins. Diagnosing
566 conditional anthropogenic contributions to heavy colorado rainfall in september 2013. *Weather
567 and Climate Extremes*, 17:1–6, 2017.
- 568 A. Pendergrass, D. Coleman, C. Deser, F. Lehner, N. Rosenbloom, and I. Simpson. Nonlinear
569 response of extreme precipitation to warming in cesm1. *Geophysical research letters*, 46(17-18):
570 10551–10560, 2019.

- 571 T. Peterson, C. Folland, G. Gruza, W. Hogg, A. Mokssit, and N. Plummer. *Report on the activities*
572 *of the working group on climate change detection and related rapporteurs*. Citeseer, 2001.
- 573 S. Pfahl, P. A. O’Gorman, and E. M. Fischer. Understanding the regional pattern of projected
574 future changes in extreme precipitation. *Nature Climate Change*, 7(6):423–427, 2017.
- 575 A. Ribes, S. Qasmi, and N. P. Gillett. Making climate projections conditional on historical obser-
576 vations. *Science Advances*, 7(4):eabc0671, 2021.
- 577 S. C. Scherrer, E. M. Fischer, R. Posselt, M. A. Liniger, M. Croci-Maspoli, and R. Knutti. Emerging
578 trends in heavy precipitation and hot temperature extremes in switzerland. *Journal of Geophysical*
579 *Research: Atmospheres*, 121(6):2626–2637, 2016.
- 580 K. Schroeder and G. Kirchengast. Sensitivity of extreme precipitation to temperature: the variability
581 of scaling factors from a regional to local perspective. *Climate Dynamics*, 50(11):3981–3994, 2018.
- 582 S. Seneviratne, X. Zhang, M. Adnan, W. Badi, C. Dereczynski, A. Di Luca, S. Ghosh, I. Iskandar,
583 J. Kossin, S. Lewis, F. Otto, I. Pinto, M. Satoh, S. M. Vicente-Serrano, M. Wehner, and B. Zhou.
584 Weather and climate extreme events in a changing climate. In Masson-Delmotte, V., P. Zhai,
585 A. Pirani, S. L. Connors, C. Péan, S. Berger, N. Caud, Y. Chen, L. Goldfarb, M. I. Gomis,
586 M. Huang, K. Leitzell, E. Lonnoy, J. B. R. Matthews, T. K. Maycock, T. Waterfield, O. Yelekçi,
587 R. Yu, and B. Zhou, editors, *Climate Change 2021: The Physical Science Basis. Contribution*
588 *of Working Group I to the Sixth Assessment Report of the Intergovernmental Panel on Climate*
589 *Change*, chapter 11. Cambridge University Press. In Press., 2021.
- 590 S. I. Seneviratne. Historical drought trends revisited. *Nature*, 491(7424):338–339, 2012.
- 591 S. Sherwood, R. Roca, T. Weckwerth, and N. Andronova. Tropospheric water vapor, convection,
592 and climate. *Reviews of Geophysics*, 48(2), 2010.
- 593 J. Sillmann, V. Kharin, X. Zhang, F. Zwiers, and D. Bronaugh. Climate extremes indices in
594 the cmip5 multimodel ensemble: Part 1. model evaluation in the present climate. *Journal of*
595 *Geophysical Research: Atmospheres*, 118(4):1716–1733, 2013a.

- 596 J. Sillmann, V. V. Kharin, F. Zwiers, X. Zhang, and D. Bronaugh. Climate extremes indices in the
597 cmip5 multimodel ensemble: Part 2. future climate projections. *Journal of Geophysical Research:*
598 *Atmospheres*, 118(6):2473–2493, 2013b.
- 599 M. Sugiyama, H. Shiogama, and S. Emori. Precipitation extreme changes exceeding moisture
600 content increases in miroc and ipcc climate models. *Proceedings of the National Academy of*
601 *Sciences*, 107(2):571–575, 2010.
- 602 Q. Sun, X. Zhang, F. Zwiers, S. Westra, and L. V. Alexander. A global, continental, and regional
603 analysis of changes in extreme precipitation. *Journal of Climate*, 34(1):243–258, 2021.
- 604 N. C. Swart, J. N. Cole, V. V. Kharin, M. Lazare, J. F. Scinocca, N. P. Gillett, J. Anstey, V. Arora,
605 J. R. Christian, S. Hanna, et al. The canadian earth system model version 5 (canesm5. 0.3).
606 *Geoscientific Model Development*, 12(11):4823–4873, 2019.
- 607 C. Tebaldi, K. Hayhoe, J. M. Arblaster, and G. A. Meehl. Going to the extremes. *Climatic change*,
608 79(3):185–211, 2006.
- 609 K. E. Trenberth. Changes in precipitation with climate change. *Climate Research*, 47(1-2):123–138,
610 2011.
- 611 N. Utsumi, S. Seto, S. Kanae, E. E. Maeda, and T. Oki. Does higher surface temperature intensify
612 extreme precipitation? *Geophysical research letters*, 38(16), 2011.
- 613 J. Vial, J.-L. Dufresne, and S. Bony. On the interpretation of inter-model spread in cmip5 climate
614 sensitivity estimates. *Climate Dynamics*, 41(11-12):3339–3362, 2013.
- 615 G. Wang, D. Wang, K. E. Trenberth, A. Erfanian, M. Yu, M. G. Bosilovich, and D. T. Parr.
616 The peak structure and future changes of the relationships between extreme precipitation and
617 temperature. *Nature Climate Change*, 7(4):268–274, 2017.
- 618 M. Wehner, P. Gleckler, and J. Lee. Characterization of long period return values of extreme daily
619 temperature and precipitation in the cmip6 models: Part 1, model evaluation. *Weather and*
620 *Climate Extremes*, 30:100283, 2020.

- 621 M. F. Wehner. Characterization of long period return values of extreme daily temperature and
622 precipitation in the cmip6 models: Part 2, projections of future change. *Weather and Climate*
623 *Extremes*, 30:100284, 2020.
- 624 S. Westra, L. V. Alexander, and F. W. Zwiers. Global increasing trends in annual maximum daily
625 precipitation. *Journal of climate*, 26(11):3904–3918, 2013.
- 626 K. Wyser, T. v. Noije, S. Yang, J. v. Hardenberg, D. O’Donnell, and R. Döscher. On the increased
627 climate sensitivity in the ec-earth model from cmip5 to cmip6. *Geoscientific Model Development*,
628 13(8):3465–3474, 2020.
- 629 M. D. Zelinka, T. A. Myers, D. T. McCoy, S. Po-Chedley, P. M. Caldwell, P. Ceppi, S. A. Klein,
630 and K. E. Taylor. Causes of higher climate sensitivity in cmip6 models. *Geophysical Research*
631 *Letters*, 47(1):e2019GL085782, 2020.
- 632 W. Zhang, G. Villarini, and M. Wehner. Contrasting the responses of extreme precipitation to
633 changes in surface air and dew point temperatures. *Climatic change*, 154(1):257–271, 2019.

Declaration of interests

The authors declare that they have no known competing financial interests or personal relationships that could have appeared to influence the work reported in this paper.

The authors declare the following financial interests/personal relationships which may be considered as potential competing interests:

Journal Pre-proof